New Mexico Geological Society

Downloaded from: https://nmgs.nmt.edu/publications/guidebooks/76



Parsing the Great Unconformity Via $^{40}Ar/^{39}Ar$ Thermal History of the Sandia Granite

Matthew T. Heizler, Karl E. Karlstrom, and Jason W. Ricketts
2026, pp. 145-158. https://doi.org/10.56577/FFC-76.145

in:

Geology of the Albuquerque Region - Fall Field Conference 2026, Connell, Sean D.; Koning, Daniel J.;, New Mexico Geological Society 76th Annual Fall Field Conference Guidebook, 452 p. https://doi.org/10.56577/FFC-76

This is one of many related papers that were included in the 2026 NMGS Fall Field Conference Guidebook.

Annual NMGS Fall Field Conference Guidebooks

Every fall since 1950, the New Mexico Geological Society (NMGS) has held an annual Fall Field Conference that explores some region of New Mexico (or surrounding states). Always well attended, these conferences provide a guidebook to participants. Besides detailed road logs, the guidebooks contain many well written, edited, and peer-reviewed geoscience papers. These books have set the national standard for geologic guidebooks and are an essential geologic reference for anyone working in or around New Mexico.

Free Downloads

NMGS has decided to make peer-reviewed papers from our Fall Field Conference guidebooks available for free download. This is in keeping with our mission of promoting interest, research, and cooperation regarding geology in New Mexico. However, guidebook sales represent a significant proportion of our operating budget. Therefore, only *research papers* are available for download. *Road logs*, *mini-papers*, and other selected content are available only in print for recent guidebooks.

Copyright Information

Publications of the New Mexico Geological Society, printed and electronic, are protected by the copyright laws of the United States. No material from the NMGS website, or printed and electronic publications, may be reprinted or redistributed without NMGS permission. Contact us for permission to reprint portions of any of our publications.

One printed copy of any materials from the NMGS website or our print and electronic publications may be made for individual use without our permission. Teachers and students may make unlimited copies for educational use. Any other use of these materials requires explicit permission.

This page is intentionally left blank to maintain order of facing pages.

New Mexico Geological Society Guidebook, 76th Fall Field Conference, 2026, p. 145–157, https://doi.org/10.56577/FFC-76.145

PARSING THE GREAT UNCONFORMITY VIA ^{40}AR/^{39}AR THERMAL HISTORY OF THE SANDIA GRANITE

MATTHEW T. HEIZLER[1], KARL E. KARLSTROM[2], AND JASON W. RICKETTS[3]

[1]New Mexico Bureau of Geology and Mineral Resources, Socorro, NM 87801; matt.heizler@nmt.edu
[2] Department of Earth and Planetary Sciences, Univ. of New Mexico, Albuquerque, NM 87131
[3]Earth, Environment and Resource Sciences, University of El Paso, El Paso, TX 79968

Abstract—The 1.453 ± 0.012 Ga Sandia granite (U-Pb age) is nonconformably overlain by ~350–300 Ma Mississippian and Pennsylvanian strata, indicating that 1.1 billion years of Earth history is "missing" (i.e., not recorded). ^{40}Ar/^{39}Ar thermochronology provides constraints on the history of basement cooling and unroofing below the unconformity. Muscovite ^{40}Ar/^{39}Ar dates of 1.45 Ga are concordant with the emplacement age of the granite, indicating intrusion at mid-crustal levels (~10 km [~6.2 mi]) with ambient temperatures near 400 °C and rapid cooling from ~650 to 400 °C at emplacement. Slower cooling (~2 °C/Myr) to 300 °C is recorded in 1.43 Ga biotite ages, suggesting that a lack of basement unroofing and overall crustal stability followed the ~1.45 Ga Picuris orogeny. Previously published K-feldspar data (n = 1) record T~275 °C at 1.2 Ga and T~250 °C at 1.0 Ga, suggesting continued very slow cooling (0.1 °C/Myr) from 1.3 to 1.0 Ga. K-feldspar MDD models indicate T~150 °C at 800 Ma, reflecting accelerated cooling (0.5–1 °C/Myr) due to exhumation to ~5 km (3.1 mi) depths (inferred from the temperature data, assuming geothermal gradients of 25-30 °C/km). Thus, approximately half of the ~10 km (~6.2 mi) of rock originally above the Sandia granite was removed between 1.0 and 0.8 Ga due to uplift of the Rocky Mountains region relative to the Great Plains during the broader Grenville orogeny. The ~5 km (~3.1 mi) "other half" of the basement was eroded between 800 and 350 Ma, but the T–t path is poorly recorded in the available thermochronometers. Basement erosion may have taken place early (800–500 Ma) or late (~350–300 Ma, during the Ancestral Rocky Mountain orogeny), or some of each. The Great Unconformity was then buried by ~5 km (3.1 mi) of post-Mississippian strata and re-heated to ~150 °C. Potassium-feldspar age spectra exhibit initial steps as young as 100 Ma, compatible with published modeled apatite fission-track and apatite (U+Th)/He data indicating that the basement below the Great Unconformity heated to ~150 °C before cooling to near-surface temperatures during uplift of the Sandia Mountains after ~20 Ma. Overall, the development of the sub-Mississippian Great Unconformity in the Sandia Mountains cannot be attributed to a single cause but rather occurred through multiple pulses of basement exhumation.

INTRODUCTION

The spectacular nonconformable contacts between Proterozoic crystalline basement and overlying sedimentary strata (Fig. 1) provide evidence for missing time and eroded rock. When the erosion occurred, how much rock was removed, and the driver(s) for basement exhumation remain incompletely known. Deep basement erosion of cratons is evident on many continents, and such Great Uniformities (Dutton, 1882) are first-order geologic phenomena.

In the Colorado Plateau–Rocky Mountains region, the overall amount of time missing (i.e., not recorded) across these contacts is well constrained by the ages of rocks above and below them. Underlying igneous and metamorphic basement rocks range are 1.84–1.60 Ga in the Grand Canyon (Karlstrom and Timmons, 2012) and 1.75–1.35 Ga in New Mexico and southern Colorado (Ricketts et al., 2021). The basal overlying subhorizontal sedimentary strata are 1.25 Ga in the Grand Canyon (Karlstrom et al., 2021), 1.30 Ga on the Great Plains of northern New Mexico (Amarante et al., 2005), and 350–150 Ma in New Mexico (Ricketts et al., 2021). In most areas, the amount of time missing at the unconformity is well over a billion years.

In the Sandia Mountains (Fig. 1), and elsewhere in the southern Rocky Mountains, 1.75–1.45 Ga crystalline basement rocks record mid-crustal tectonism that built mountain ranges during several episodes of plate convergence (Whitmeyer and Karlstrom, 2007). The Sandia granite itself was intruded into deforming metamorphic rocks at 1.45 Ga (Kirby et al., 1995; Holland et al., 2020). Strata above the nonconformity comprise 350–300 Ma Mississippian and Pennsylvanian sedimentary rocks deposited during the Ancestral Rocky Mountain orogeny (Leary et al., 2017). Cambrian to Mississippian strata are present elsewhere in the region but were either not deposited or were eroded in northern New Mexico (Amato and Mack, 2012).

Given the variable ages of rocks below and above the Great Unconformities, additional thermochronology-based studies can help resolve the missing time. This paper explores the history of erosion of the Sandia granite via the temperature–time (T–t) path the crystallized pluton took from the middle crust to Earth's surface. This is investigated via ^{40}Ar/^{39}Ar analyses of muscovite, biotite, and K-feldspar, minerals with different closure temperatures, which can constrain parts of the T–t path. This thermal history is then approximately converted to paleodepth using an assumed geothermal gradient of ~30 °C/km to reconstruct the exhumation history.

SANDIA GRANITE SAMPLING AND ^{40}AR/^{39}AR METHODS

Figure 2 shows the distribution of samples of the Sandia granite, pegmatites, and aureole rocks reported in this paper and Table 1 lists sample types and minerals analyzed. The

megacrystic main unit of the pluton has yielded a LA-ICPMS U-Pb zircon date of 1453 ± 12 Ma (Holland et al., 2020). Biotite-bearing samples K1, K4, K6, and K10 are from the megacrystic main unit of the pluton, whereas sample K5 is from a finer-grained biotite-rich dike. Muscovite samples are primarily from pegmatites with K7 crosscutting the 1.65 Ga Cibola gneiss of the southern part of the pluton's aureole and K2 a boudinaged pegmatite in the northern aureole. Pegmatites

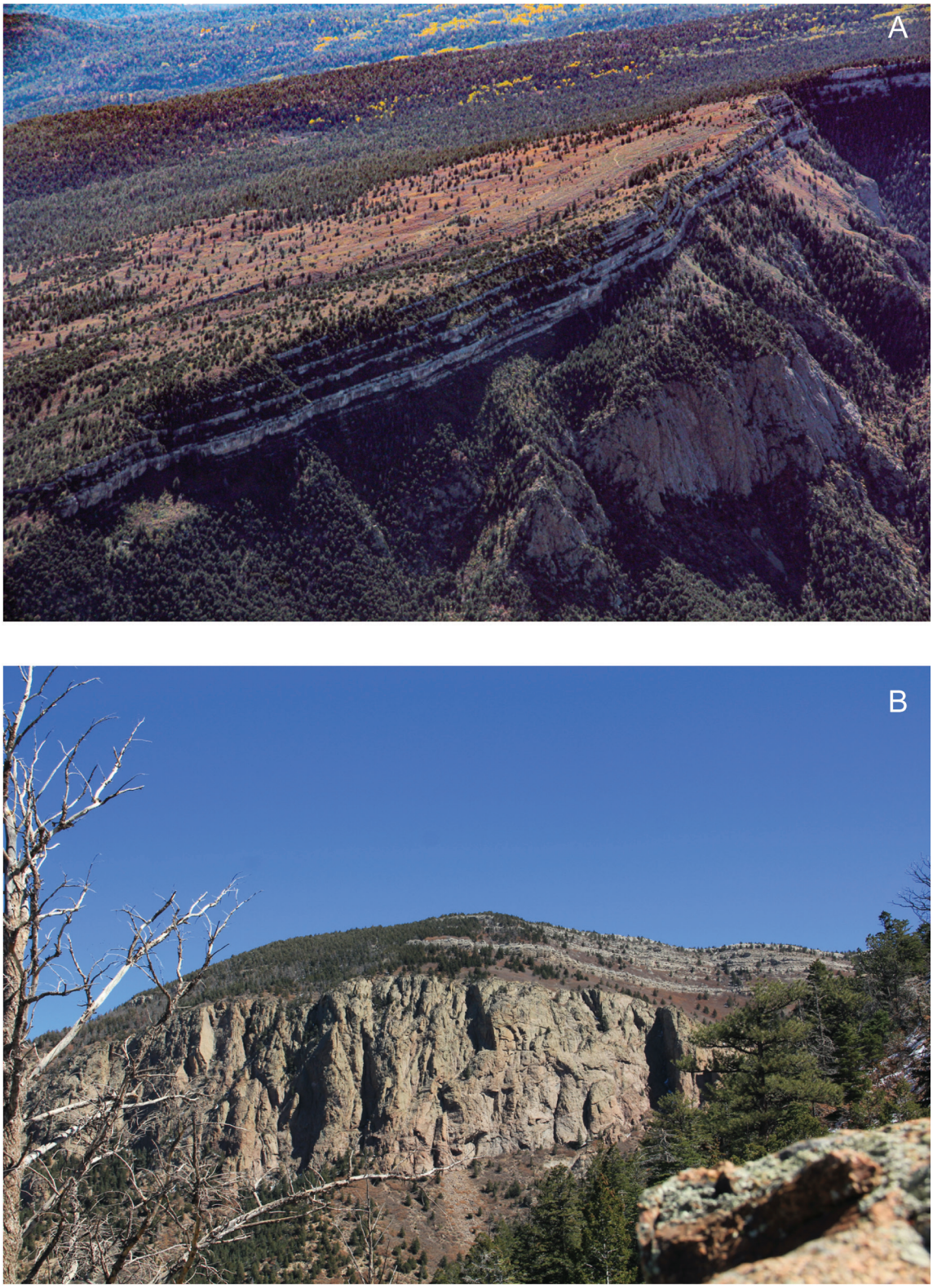


FIGURE 1. Views of the Great Unconformity: a) looking south at the east-side dip slope; the Great Unconformity is at the base of the tree-covered slope in Sandia Formation with Madera Group (Gray Mesa Formation) limestone forming much of the dip slope; b) looking east from La Luz trail; Sandia granite in cliff below the Middle Pennsylvanian Sandia Formation.

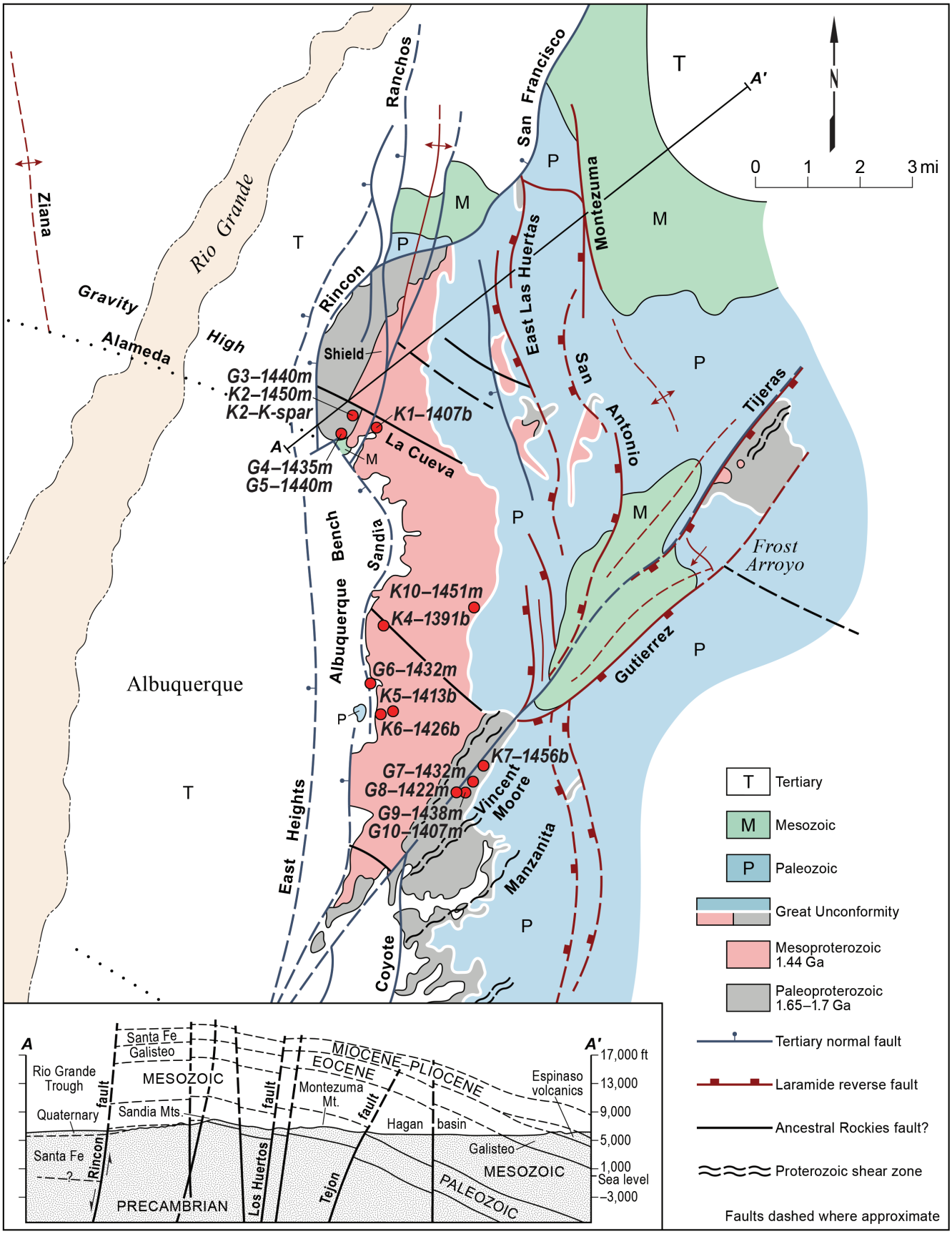


FIGURE 2. Sample location map for Ar-Ar samples from the Sandia granite and its aureole keyed to Table 1. Cross-section A-A' (from Kelley and Northrop, 1975) shows ~5 km (~3.1 mi) of Phanerozoic strata of the Hagan Basin that are inferred to have covered the Sandia Mountains area until ~20 Ma. U-Pb zircon LAICPMS zircon age for the Sandia granite of 1453 ±12 Ma is from Holland et al. (2020).

TABLE 1. Summary of $^{40}Ar/^{39}Ar$ results.

Sample	Latitude(°)	Longitude(°)	Rock Type/Location	Min	n	$\%^{39}Ar$	Age±1σ (Ma)
K1	35.213417	-106.475628	Sandia granite La Luz trail (at Tramway cutoff)	B	2	27.8	1407.2±2.1
K2	35.215313	-106.48866	Pegmatite-Juan Tabo near La Cueva Trailhead	M	4	37.6	1450.4±2.1
K2*	35.215313	-106.48866	Pegmatite-Juan Tabo near La Cueva Trailhead	K	35	100.0	1073.3±2.0
K4	35.136191	-106.475056	Sandia granite, Coarse, main phase - Embudo Trail	B	1	21.7	1390.7±1.6
K5	35.100314	-106.471459	Fine-grained granite dike, Embudo Cyn.	B	1	40.4	1413.1±1.5
K6	35.098681	-106.475258	Sandia granite across from water tank, Embudo Cyn.	B	1	11.3	1425.6±1.4
K7	35.068928	-106.428553	Pegmatite in coarse Cibola gneiss, Tijeras Cyn.	M	4	24.1	1455.9±4.5
K10	35.14224	-106.430788	Sandia granite- Coarse, foliated interior of pluton	B	1	29.4	1450.9±2.1
G2	35.215174	-106.488984	Pegmatite - Juan Tabo area	M	3	23.5	1438.1±1.5
G3	35.215237	-106.488922	Pegmatite - Juan Tabo area	M	2	17.2	1440.0±2.7
G4	35.20903	-106.493178	Pegmatite - Juan Tabo area	M	4	26.5	1434.7±1.2
G5	35.20903	-106.493178	Juan Tabo Schist crosscut by G4 pegmatite	M	2	27.9	1429.3±3.2
G6	35.111381	-106.48555	Pegmatite - Piedra Lisa trail	M	4	24.1	1432.0±1.1
G7	35.067022	-106.429649	Pegmatite crosscutting Cibola gneiss, Tijeras Cyn.	M	19	84.8	1431.8±1.3
G8	35.06702	-106.429289	Pegmatite crosscutting Cibola gneiss, Tijeras Cyn.	M	1	15.3	1422.4±1.7
G9	35.066318	-106.425798	Pegmatite crosscutting quartzite, Seven Springs shear	M	15	97.5	1438±0.93
G10	35.066318	-106.425798	Micaceous quartzite crosscut by G9 pegmatite	M	4	36.8	1406.6±1.8

Notes: L# - Lab identifier; Min—B=Biotite, M=Muscovite, K=K-feldspar; Plateau age—Inverse variance weighted mean of selected age spectrum steps or single step; $\%^{39}Ar$—% of ^{39}Ar comprising steps used for reported age; n—number of heating steps used for age calculation; and * —Reported age is the integrated age.

similar to K2 are G2, G3, and G4 from a set of relatively undeformed NW-striking pegmatite dikes that crosscut high-grade Juan Tabo schist in the northern part of the pluton aureole (Fig. 3). G5 is a relatively fine-grained sample of muscovite-bearing Juan Tabo schist collected at the same location where G4 pegmatite cuts the schist. Here, both fine- and coarse-grained muscovite can be used to test a possible correlation between closure temperature and physical grain size (cf. Hodges et al., 1994; Harrison et al., 2009). Samples G6–G9 are pegmatites from more southerly exposures in the Sandia Mountains, and G10 is from the same location as G9 and is a fine-grained quartzite. Potassium feldspar was also extracted from sample K2.

The dated minerals are single whole crystals or crystal fragments (ranging from 0.2-to 4-mm in diameter) that were either plucked directly out of the rock or extracted from coarsely crushed rock. The K-series samples were irradiated in the NM-188 package for 100 hours at the McMaster University reactor in Hamilton, Ontario, and the G-series for 64 hours at the U.S. Geological Survey (USGS) reactor in Denver, Colorado. All samples were step-heated in a temperature-controlled double-vacuum Mo-furnace, and argon isotopes were measured with a MAP-215-50 mass spectrometer. All ages are reported relative to Fish Canyon sanidine with an assigned age of 28.201 Ma (Kuiper et al., 2008) and a total ^{40}K decay constant of $5.463 \times 10^{-10}/a$ (Min et al., 2000). Detailed analytical methods and argon results are provided in the Appendix.

RESULTS

Between 9 and 32 step-heating increments were performed on the 11 muscovite and 5 biotite samples to obtain $^{40}Ar/^{39}Ar$ age spectra (Figs. 4 and 5). A K-feldspar age spectrum was generated using 35 heating steps (Fig. 6a). The muscovite age spectra are mostly from pegmatites and have steep age gradients between about 1300 and 1400 Ma for the initial 2–10% of the age spectra before showing overall flat age patterns for the remaining part of the spectra (Fig. 4a–f and h). Two of the spectra initially record old apparent ages for the first few percent of gas released, then step down and yield flat segments with plateau ages of 1440–1430 Ma (Fig. 4g and i). Although the muscovite spectra are somewhat flat, they commonly gently rise across the spectrum; thus, the final 20–40% of each spectrum is used to derive a terminal age correlated with the onset of partial argon retention. Muscovite samples G5 and G10 are from schist and quartzite, respectively, and especially for G10 are somewhat younger than the coarser-grained muscovite from the pegmatites (Fig. 4e and i).

Biotite samples yield somewhat chaotic age spectra and commonly show a "crankshaft" pattern with the oldest steps near the middle of the release patterns (Fig. 5a–e). Individual steps range from about 1450 to 1200 Ma, with the oldest intermediate part of each spectrum having preferred dates between about 1450 and 1390 Ma; this date is equated with the onset of argon retention. The integrated ages of biotite are about 60–10 Ma younger than the preferred dates.

The K-feldspar age spectrum has a very steep age gradient from about 100 to 1000 Ma over the first 5% of gas released, followed by a near flat segment at ~1000 Ma for the next 40%

of the spectrum (Fig. 6A). Over the final 50% of gas released, ages rise from about 1050 Ma to a terminal value at ~1200 Ma. This 1200 Ma date records the initiation of argon retention in the K-feldspar, corresponding to a large diffusion-domain closure temperature of ~275 °C. The K-feldspar spectrum and the extraction of a thermal history from the data are discussed further below.

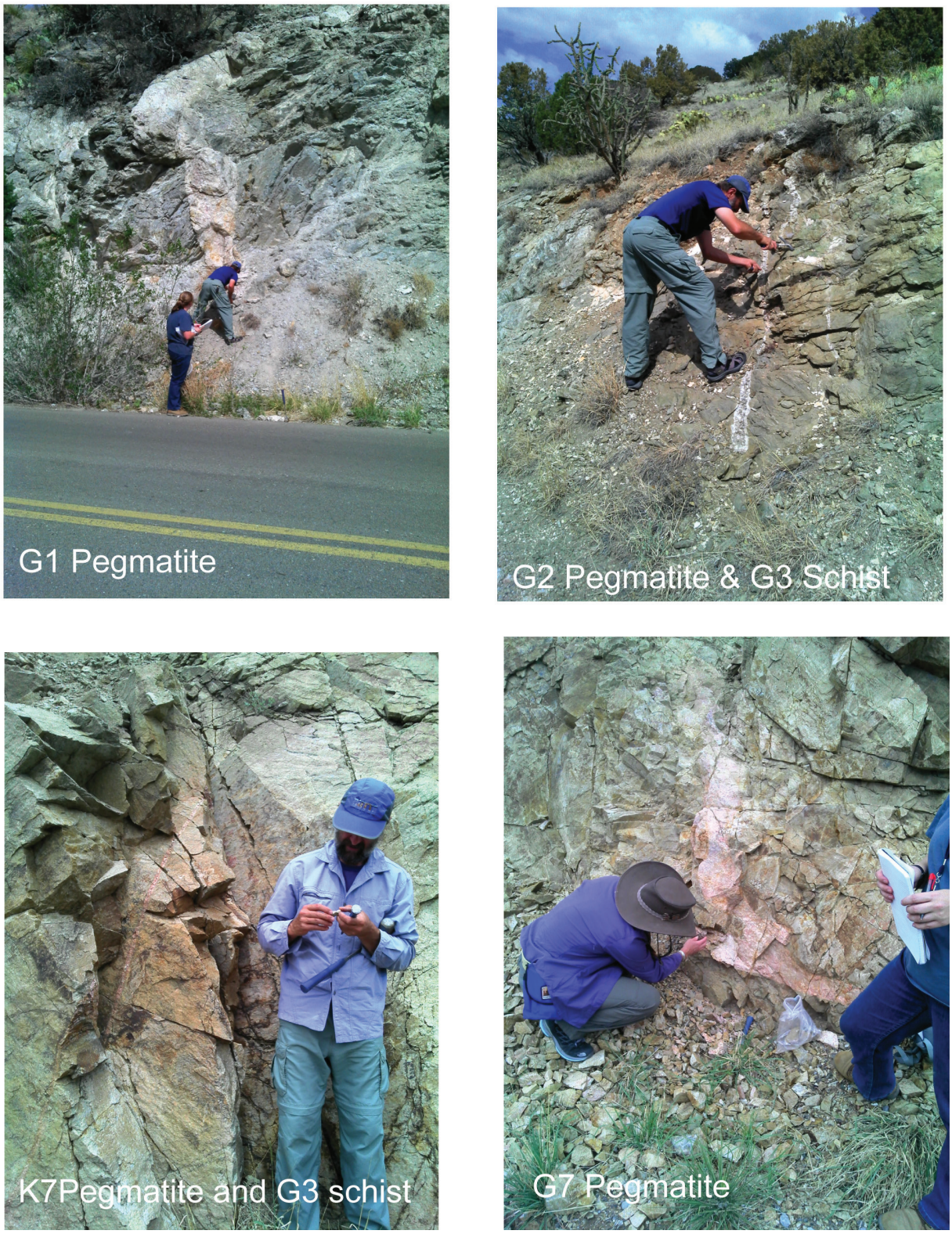


FIGURE 3. Photographs of dated samples. Pegmatites G1, G2, and K7 crosscut the Juan Tabo schist (G3) along the road near Stop 1 of the Day 1 roadlog. Pegmatite G7 crosscuts the Seven Springs shear zone within the southern metamorphic aureole of the Sandia granite. Muscovite ages of ~1450–1430 Ma are interpreted to represent the timing of pegmatite crystallization.

Figure 6B shows potential thermal histories based on multiple diffusion domain (MDD) analysis of K-feldspar (cf. Lovera et al., 1989). K-feldspars commonly have a lower argon closure temperature than micas, and thus, as shown here, K-feldspar will yield much younger dates than micas. K-feldspar can also reveal complex internal age profiles and, when

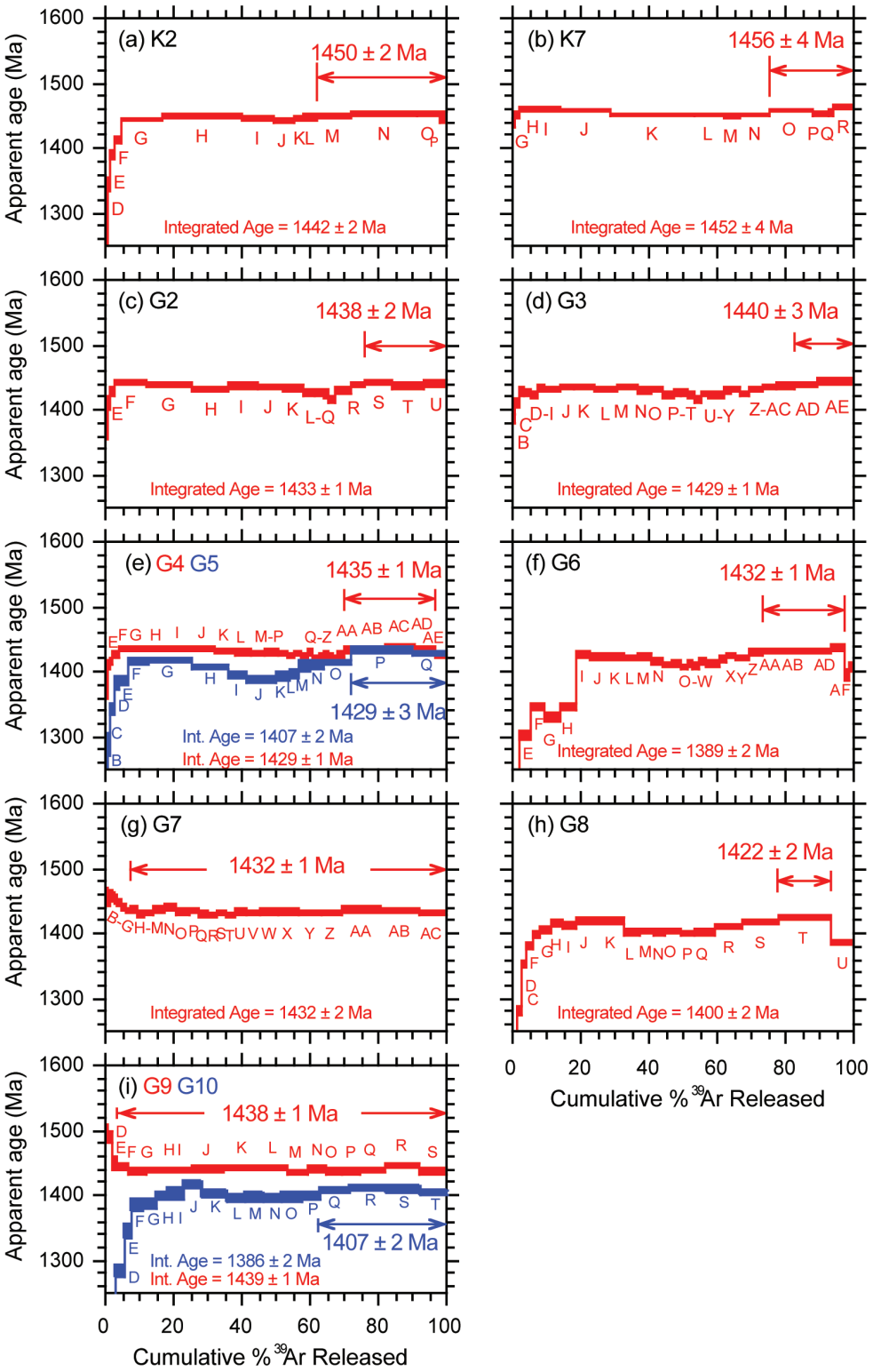


FIGURE 4. Muscovite age spectra for leucocratic rocks associated with the Sandia granite (red) and metamorphic country rocks (blue). Most of the spectra are from 1–3 mm diameter single crystals. Plots e and i: Samples G5 and G10 are finer-grained (0.2–0.5 mm) muscovite from host rock that are crosscut by G4 and G9, respectively, which are coarse-grained pegmatites. Most spectra show age discordance with commonly initially climbing patterns rising to a terminal age that records cooling below about 375 °C. Most terminal ages are greater than 1430 Ma, with samples K2 and K7 yielding dates near 1450 Ma, which are concordant with the emplacement age of the Sandia granite.

coupled with argon kinetic parameters derived from the release of ^{39}Ar during step-heating analysis, yield insights into the details of the thermal history. The MDD detailed methodology is described in Sanders et al. (2006) and Rickets et al. (2021).

Potassium-feldspar is partitioned into variable diffusion length scales related to their complex microtextures and because diffusion length scale is a parameter that defines closure temperature, a sample can typically constrain the thermal history between about 275 °C and 150 °C. Thus, unlike micas, the closure temperature distribution can be measured (rather than inferred) for each analysis and used to construct two main types of thermal histories. One type of thermal history is based on cooling only models (constrained, yellow polygon) and in this case the temperature path goes through about 275 °C at 1200 Ma, where it then records very slow cooling to about 240 °C by 1000 Ma and then accelerated cooling to about 150 °C by ~800 Ma (Fig. 6b). In order to generate the very steep age gradient at the beginning of the age spectrum that gets as young as 100 Ma, a cooling only model would require residence near 150 °C between 800 and 100 Ma. However, this extension of the cooling-only thermal model is not shown because we know that the Mississippian (Great Unconformity) was exhumed to the surface, followed by Mesozoic burial; thus, a cooling-only model for this time period is not geologically relevant here.

The second type of thermal history analysis is an unconstrained model, in which the sample is allowed to heat and cool, as shown by the multiple gray lines in Figure 6b. There are numerous, but similar, potential T–t paths for the unconstrained thermal histories; however, they have important convergence regions. Similar to the constrained cooling-only paths, the thermal history is near 300 °C just prior to about 1200 Ma and then it can cool to variable temperatures between 1200 and 1000 Ma, but it must return to about 250 °C between 900 and 1000 Ma in order to match the measured age spectrum shape (red modeled spectra, Fig. 6a). Between 1000 and 800 Ma, the two models are very similar. The unconstrained models are nearly continuously required to return to ~150 °C until less than 100 Ma to yield the steep initial age gradient of the measured age spectrum. Like the constrained models, these models are not geologically relevant for this time period.

DISCUSSION

Figure 7 and Table 1 summarize the preferred ages of muscovite and biotite. The yellow polygon shows the U-Pb zircon

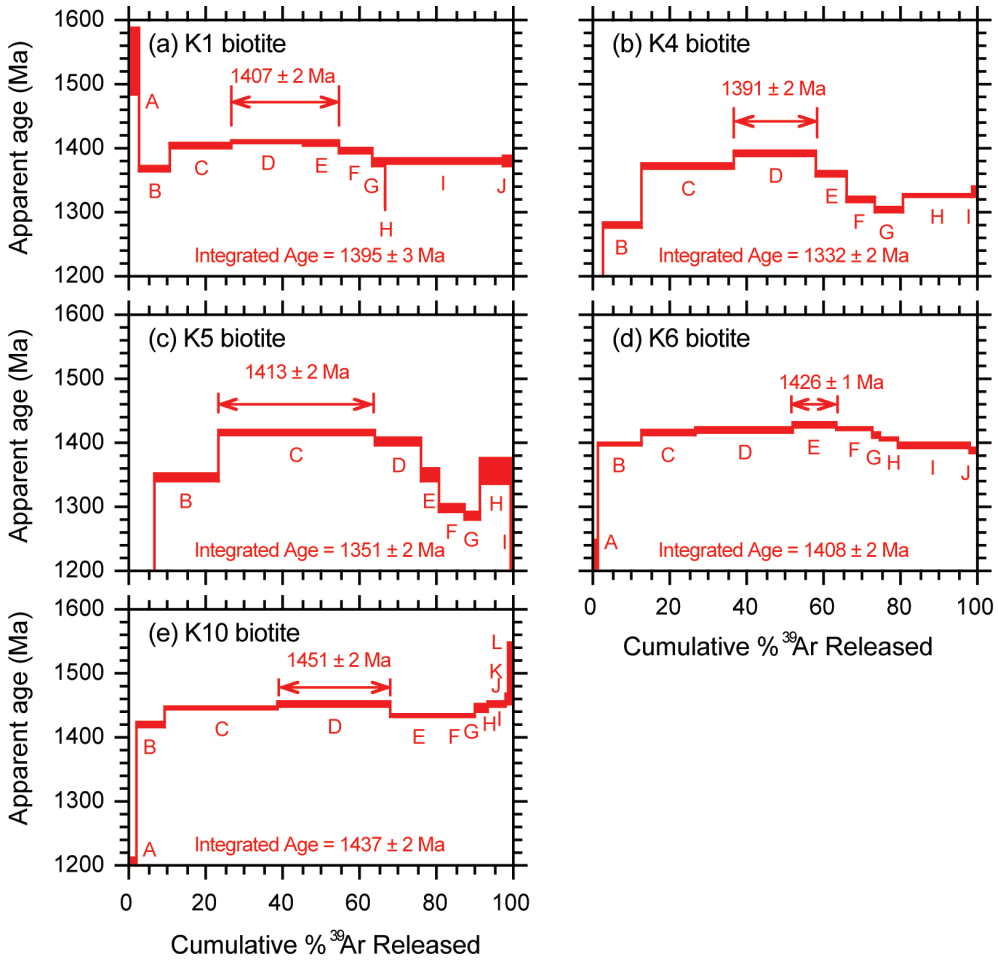


FIGURE 5. Biotite from Sandia granite and associated dike rocks (a–e). Biotite spectra are disturbed, and the oldest steps of the spectra range between 1451 Ma and 1407 Ma. The complexity likely results from nonhomogeneous degassing of individual crystals containing complex age zoning related to long-term residence (>100 Ma) at temperatures between 275 and 325 °C.

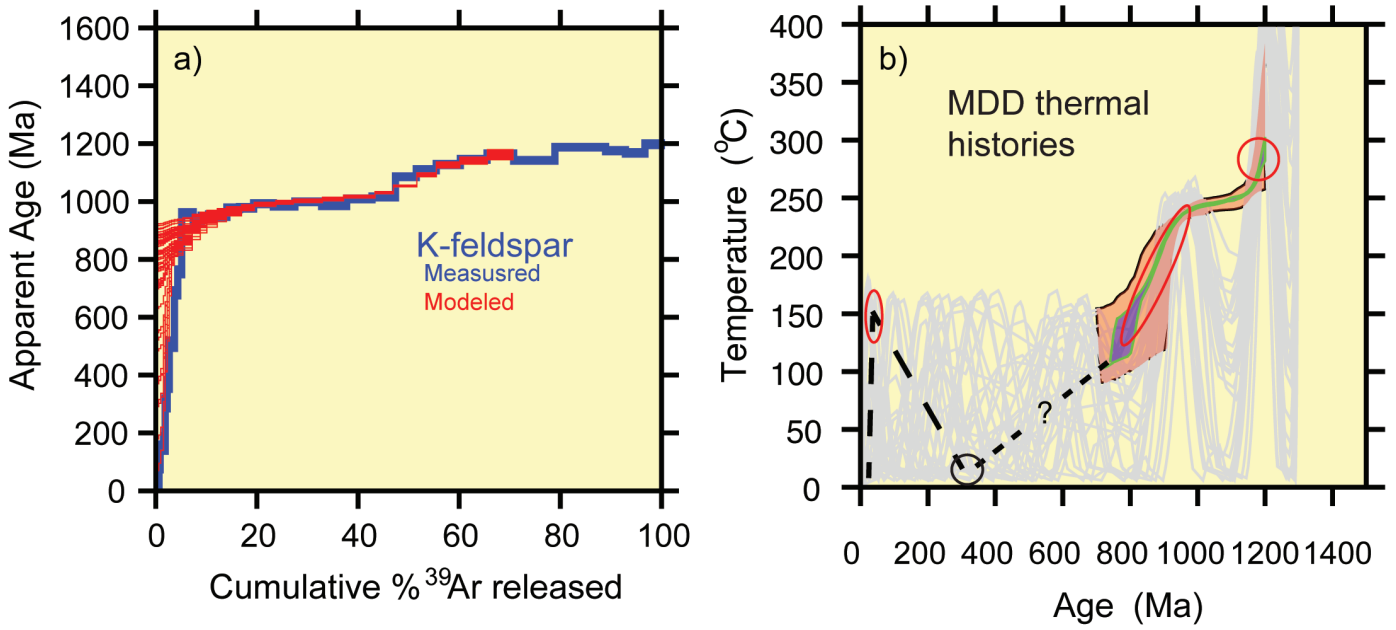


FIGURE 6. a) Potassium-feldspar measured age spectrum (blue) and multiple diffusion domain (MDD) derived model age spectra (red). Model spectra obtained by forward integration of thermal histories yield age spectra that match the measured spectrum. b) K-feldspar MDD-derived thermal histories are shown as gray lines (unconstrained) and a solid pale red and green polygon (cooling only). Unconstrained thermal histories allow for cooling and reheating. The K-feldspar thermal histories require temperatures near 275 °C at 1200 Ma and 250 °C between 1000 Ma and 900 Ma with moderately rapid cooling to 150 °C by ~800 Ma. Red ellipses are temperature–time (T–t) regions that are best constrained by the K-feldspar data. The MDD model does not directly constrain the 800–100 Ma time interval, except that temperatures cannot significantly exceed 150 °C. The very steep initial age gradient, with a youngest K-feldspar date near 100 Ma, requires temperatures near 150 °C post-100 Ma. Dashed lines are T–t trajectories indicating unknown cooling paths prior to erosion to the surface by 350 Ma to 300 Ma and subsequent heating during Mesozoic and Cenozoic sedimentation.

date and uncertainty (1453 ± 12 Ma, 2σ, Holland et al., 2020) of the crystallization age of the Sandia granite, and even without considering the ^{40}K decay constant error for the argon data, two muscovite dates (samples K2 and K7) are analytically indistinguishable from the crystallization age. Seven of the next youngest muscovite groups, between 1430 and 1440 Ma, are distinctly younger than the emplacement age of the Sandia granite. The youngest coarse-grained pegmatitic muscovite is from G8 with an age near 1420 Ma.

Samples G5 and G10 are relatively fine-grained (0.5–1 mm and 0.2–0.5 mm, respectively) and are country rock samples intruded by G4 and G9 pegmatites, respectively. For the G4 and G5 pair their dates are nearly the same (Table 1) and if argon retention is correlated to physical grain size (cf. Hodges et al., 1994; Harrison et al., 2009), the age concordance of coarse and fine muscovite would indicate fairly rapid cooling between the two discordant closure temperatures, and/or that the pegmatite date could equal the pegmatite emplacement age. That is, a higher closure temperature phase (coarse muscovite) would record an emplacement age if the pegmatite was intruded into country rock that was below the closure temperature of the pegmatitic muscovite. It appears that the finest-grained sample, G10 at ~1407 Ma, has a similar closure temperature to the coarse-grained biotite samples. The pegmatite pair G9, at 1438 Ma, is much older, and although this age could record protracted cooling between 1450 and 1438 Ma, as in G4, we suggest that the 1438 Ga date reflects the emplacement of G9.

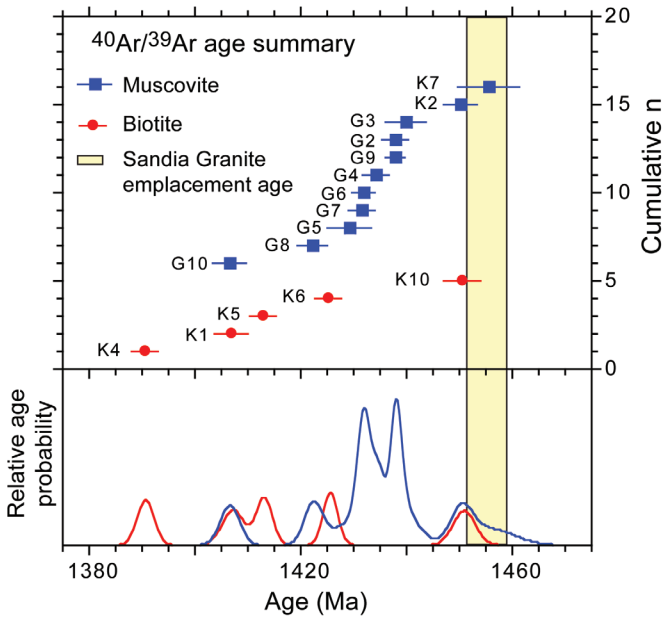


FIGURE 7. Summary of ^{40}Ar/^{39}Ar muscovite and biotite dates. Two muscovite ages are subequal to the age of the Sandia granite (yellow polygon) and indicate rapid (1–3 Ma) conductive cooling from magmatic temperatures to about 400 °C. Younger ages cluster near 1430 Ma and could represent pegmatite emplacement ages or grains with slightly lower closure temperature. Biotite ages are generally younger, reflecting their somewhat lower closure temperature (nominally 300 °C) compared to muscovite (375 °C).

The biotite ages shown in Figure 7 range from about 1450 to 1390 Ma. Due to the complexity of the biotite age spectra, there is ambiguity in choosing the oldest date in the spectrum to record the onset of argon retention, and therefore, some of this dispersion could stem from uncertainty in choosing the preferred date of the biotite. However, based on Dodson's (1973) closure temperature theory, the time of retention of the daughter product (argon in this case) can correspond to the integrated age of the biotite. The integrated ages of the biotite are also highly dispersed, suggesting either significant variation in the local thermal history (unlikely) or variation in the closure temperature of individual biotite samples. We further develop the interpretation of the dispersed biotite dates in the discussion section.

^{40}AR/^{39}AR THERMAL HISTORY OF THE SANDIA GRANITE

The combined $^{40}Ar/^{39}Ar$ data constrain large segments of the thermal history of the Sandia granite from 1450 Ma to less than 100 Ma (Fig. 8). For muscovite and biotite, we pair their apparent ages with nominal closure temperatures of 400 °C and 300 °C, respectively, based on published argon kinetic data from Harrison et al. (2009), Harrison et al. (1985), and Grove and Harrison (1996). The oldest muscovite dates from samples K2 and K7, which are about 1450 Ma, are indistinguishable from the emplacement age of the granite. This indicates that the granite cooled from magmatic temperatures to below ~400 °C within the age uncertainties (a few million years). Rapid cooling in this temperature range indicates that the granite was emplaced into ambient country rock at or below ~400 °C, resulting in cooling to ambient conditions (below muscovite closure) by conduction over a short period (cf. Heizler et al., 1988). The age probability plot shows that muscovite dates in pegmatites cluster near 1430 Ma (Fig. 7). These could have multiple interpretations. One explanation is that these muscovites have lower closure temperatures and/or these locations have experienced more protected cooling; this is unlikely since all of these muscovites are coarse-grained (1–5 mm), which seems to preclude lower closure temperature as a function of grain size and also both 1450 and 1430 Ma muscovites occur very proximal to each other and would apparently rule out variable thermal histories because of small lateral distances between samples. Our preferred explanation is that the ~1440 to 1432 Ma muscovites provide crystallization ages for pegmatites that crosscut the deformation fabrics and represent a discrete younger magmatic episode that postdated the emplacement of the Sandia granite. A caveat for this interpretation is the U-Pb age uncertainty of ±12 Ma and geologic uncertainty (rather than analytical uncertainty), where variations in muscovite ages between 1450 and 1430 Ma might reflect differences in elevation and different parts of the cooling pluton.

The biotite age spectra (Fig. 5) are significantly more complex than the muscovite age spectra, and thus, there is ambiguity for their age assignment. Choosing the oldest step from each spectrum yields a wide range of apparent ages of 1450 to 1390 Ma (Fig. 7). The integrated dates also span more than 100 Myr (1440 to 1330 Ma), and it is likely that this is a consequence of variable biotite closure temperature, coupled with long residence in this closure-temperature window. Both composition and grain size can affect biotite closure temperature, and there may be as much as 50 °C variation in moderately coarse (~200–2000 μm) crystals. Thus, it appears that the Sandia granite resided near 300 °C for a protracted period between about 1400 and 1300 Ma (Fig. 8).

The K-feldspar-derived thermal history is compatible with the mica data, as the oldest dates in the age spectrum at about 1200 Ma are younger than the micas and have a closure temperature of about 275 °C. As shown in Figure 6, previously published K-feldspar data (Ricketts et al., 2021) provide detailed segments of the thermal history (rather than a single point in T–t space) between about 150 °C and 275 °C and, in this case, yield important details of the Precambrian thermal history. Based on cooling-only models, there is a period of cooling from about 300 to 250 °C between ~1200 and 1150 Ma, followed by residence at 250 °C until about 1000 Ma, and then linear cooling to 150 °C by 800 Ma. Due to its minimum closure temperature of 150 °C and reheating in the Cenozoic, the K-feldspar data cannot record a detailed thermal history between 800 Ma and the Mississippian. It also cannot record details of basement heating during post-Mississippian burial, but because a small portion of the initial steps of the age spectrum yields dates as young as ~100 Ma, the basement below the unconformity was heated to about 150 °C. Because the youngest preserved strata in the Hagan Basin (i.e., Espinaso Formation) are about 30 Ma, the basement reached peak temperatures of 150 °C in the mid-Tertiary. AFT and AHe data (blue ellipse) indicate temperatures near 100 °C at 20 Ma, with cooling to near-surface conditions by about 10 Ma (Ricketts et al., 2016).

Alternative (unconstrained) K-feldspar models allow for cooling and heating to occur in episodes that may or may not be geologically relevant. For instance, these models allow the initial cooling, which began at 1200 Ma, to continue to much lower temperatures than cooling-only models, provided that the basement is again reheated to about 225–250 °C between 1000 and 900 Ma. Both models support a protracted period of overall cooling between about 1000 and 800 Ma. The multiple reheating models that reach about 150 °C for times less than 800 Ma are simply a consequence of the age spectrum having initial dates as young as 100 Ma and have no specific geological meaning.

Argon data provide important constraints on some segments of the cooling history of the Sandia granite (Fig. 8). Well-constrained intervals are shown with red ellipses for the K-feldspar data, a green ellipse for the biotite, and a magenta ellipse for the muscovite. The circle near 320 Ma at surface temperature is an important geological constraint represented by the sub-Mississippian unconformity. Alternative unconstrained cooling paths highlighted by dashed lines in Figure 8, which allow cooling and reheating, can satisfy the Ar data as follows.

In Figure 8, points 1) and 2), in the Great Plains, a drill hole in northern New Mexico (Amarante et al., 2005), 1.33 Ga quartz diorite was unroofed to the surface before 1.308 Ga

deposition of the Debaca Group; 1.3–1.25 Ga was also a major basement erosional event in the Grand Canyon (Timmons et al., 2012; Thurston et al., 2024) that may have been regionally significant. However, the Debaca Group thickness is only 450 m (1,476 ft), and other data suggest that the Rocky Mountains were elevated relative to the Great Plains by Mesoproterozoic and Neoproterozoic faulting along the east side of the Rocky Mountains and that the Rocky Mountains may have received no Mesoproterozoic sediment (Sanders et al., 2006). Even if Sandia granite basement was partially unroofed at 1.3–1.2 Ga, deposition of 450 m (1,476 ft) thick Debaca Group would not be sufficient to explain reheating to 250 °C by 1.1 Ga as required by the K-feldspar data. Elevated geotherms related to the southwest large igneous province (SW LIP) and passage of the New Mexico region over a plume (Mohr et al., 2023) may have caused additional reheating, but it seems unlikely that the samples could be reheated to 250 °C solely by the combination of Debaca Group sedimentation and elevated heat flow given what we know about the 1.1 Ga intrusive gabbro/diabase distribution in New Mexico.

In Figure 8, point 3), Keller et al. (2019) proposed that global-scale basement unroofing of continents occurred during one or both Snowball Earth episodes spanning 720–650 Ma. This was proposed to have resulted in several kilometers of basement removal due to glacial erosion. The argon K-feldspar data support this interpretation.

In Figure 8, point 4), no Cambrian strata are preserved in northern New Mexico, which may have been emergent during the Sauk transgressions (Karlstrom et al. 2018) due to the Trans-continental arch (Amato and Mack, 2012). However, detrital zircon data in Lower Cambrian strata from the Grand Canyon appear to have been sourced in part from the Trans-Oklahoma rift, Florida Mountains of southern New Mexico, and Wet Mountains of Colorado (Holland et al., 2024), such that the nature and continuity of the Trans-continental arch remain unknown.

In Figure 8, point 5), even if Cambrian–Devonian strata were deposited in the Sandia Mountains region, the thickness was likely less than 500 m (1,640 ft) based on preserved

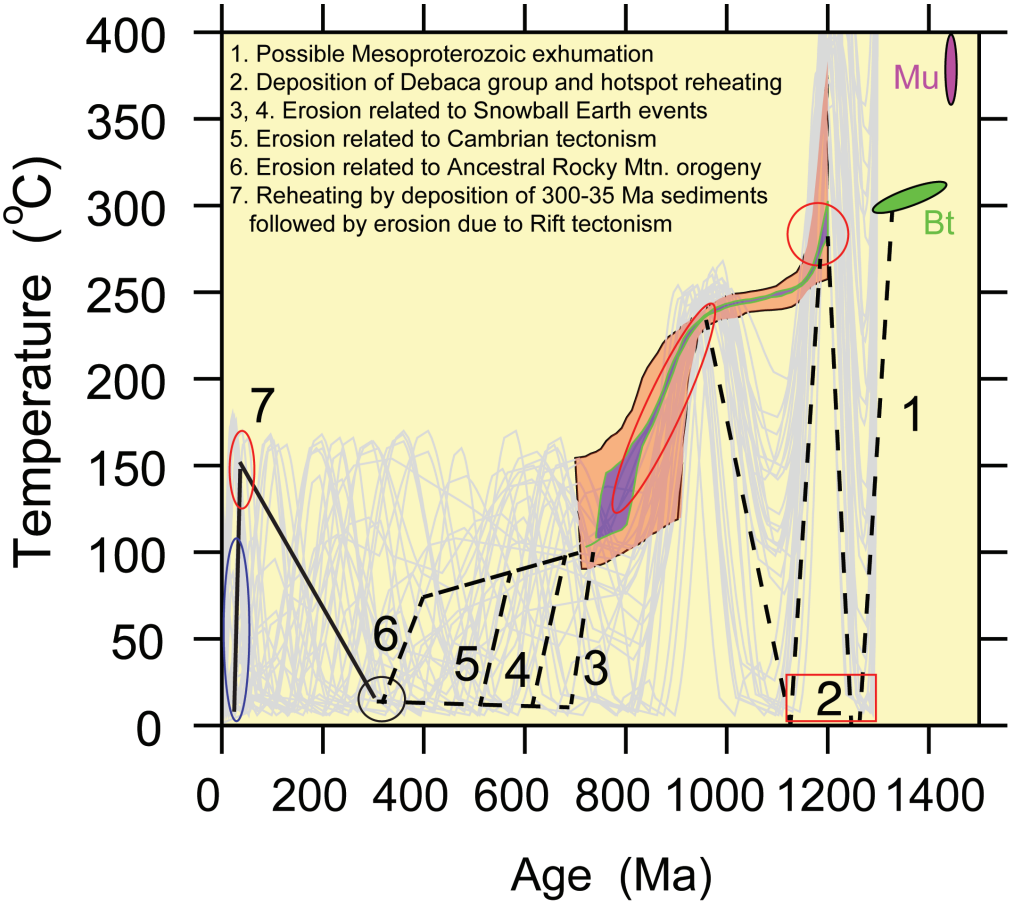


FIGURE 8. Summary of the Sandia granite thermal history based on argon, apatite fission-track (AFT), apatite (U-Th)/He (AHe) thermochronology and geological constraints. Argon-muscovite records rapid cooling from magmatic temperatures to below ~400 °C at 1.45 Ga related to the emplacement of granite at about 10 km into country rock residing at ~350 °C. Biotite, with a range of dates between 1.45 and 1.39 Ga, suggests residence near 300 °C for a protracted time interval with continued slow cooling to about 275 °C by 1200 Ma, as constrained by K-feldspar MDD cooling-only models. These models also indicate a temperature near 250 °C by ~1000 Ma, followed by accelerated cooling to 150 °C by 800 Ma. The argon data do not constrain the T–t between 800 Ma and 100 Ma; however, post-100 Ma, the granite warmed to ~150 °C due to burial. The most robust segments of the T–t path derived from the K-feldspar models are shown with red ellipses. Final cooling below 100 °C occurred after ~20 Ma, with cooling to near surface conditions by ~10 Ma based on Rickets et al. (2016) AFT and AHe data (blue ellipse). Unconstrained K-feldspar MDD models (gray lines) show other possible thermal histories, and dashed numbered lines are potential alternative thermal histories derived from geological information. The numbered segments are discussed in the text.

regional thickness trends. Thus, any lower Paleozoic reheating would have been minor.

In Figure 8, points 6) and 7), the geologic constraint of Mississippian/Pennsylvanian strata above the Great Unconformity anchors the T–t path (Fig. 8). Subsequent deposition of Phanerozoic strata to a cumulative thickness of ~5 km (~3.1 mi) is well recorded in the adjacent Hagan Basin (Fig. 2). These strata were deposited near sea level in the Paleozoic and Mesozoic, which caused progressive reheating of the underlying basement. Progressive uplift of the Great Unconformity and Phanerozoic strata above sea level began regionally in the Laramide 90–45 Ma, but the basement rocks of the Sandia Mountains were around 150 °C at 20 Ma based on both the K-feldspar and apatite thermochronology. Thus, exposures of the Great Unconformity at Sandia Crest reached their present elevation of 2 km (1.2 mi) after ~20 Ma (Ricketts et al., 2016).

COMPARISON TO OTHER THERMOCHRONOLOGY MODELS

Our reported $^{40}Ar/^{39}Ar$ muscovite, biotite, and K-feldspar data provide a detailed estimate of portions of the Sandia granite's thermal history; however, other data sets can also be incorporated and evaluated. For instance, the muscovite and biotite age spectrum data reported here may be limited by a lack of direct knowledge of the internal age distribution within a given crystal. Based on diffusion theory and knowledge of diffusion length scales, it is predicted that minerals that have resided for long durations near their closure temperature and/or have experienced complex thermal histories that have variably disturbed the spatial distribution of radiogenic argon will exhibit internal variation in apparent ages. In the simplest case, young dates would be predicted near the edge of a grain, and dates would become progressively older towards the middle of the grain. Normal step-heating methods like those used here can obscure details of the internal age distribution and potentially lead to erroneous interpretations of the thermal history.

Hodges et al. (1994) showed that muscovite and biotite crystals from samples interpreted to have undergone slow cooling have highly variable within-grain age distributions. This was determined by measuring argon compositions in gas released from ~200-µm diameter laser-probe melt pits with known geometry within the crystal. These widely variable dates were not evident in age spectra derived by more conventional step-heating approaches of the same samples.

In situ laser-probe argon data for muscovite and biotite crystals from the Sandia granite were reported by Dotson (1994). Spot analysis of 1–3 mm diameter crystals (3 biotite, 2 muscovite) yields variable dates within the grains, with one biotite grain spanning ~1250–800 Ma (Figure 9). Muscovites show a more restricted range between about 1.4 and 1.3 Ga. By calculating argon closure temperatures at the rim and core of each grain and associating young dates with the low closure temperature rim and older dates with the higher closure temperature core, Dotson (1994) derived linear-cooling trajectories.

The muscovite crystals yield cooling from about 400 to 350 °C between about 1400 and 1350 Ma, which is similar to the muscovite data from this study, but overall, about 50 Myr younger (Figs. 8 and 9). Dotson's (1994) biotite data suggest long-term residence between about 325 and 290 °C from 1300 Ma to as young as ~800 Ma. Temperatures near 300 °C prior to ~1250 Ma are compatible with the K-feldspar MDD-derived thermal histories, but spot dates as young as 800 Ma, indicating a temperature near 300 °C, are about 50 °C hotter than the MDD results.

As with all thermochronometers, there are a variety of uncertainties, especially those associated with the closure temperature estimate. For K-feldspar MDD data, the choice of the argon diffusion activation energy is the most critical parameter, and it is not always well determined from the measured data. Increasing the K-feldspar model activation energy from 46 kcal/mol used in this study to 50 kcal/mol would shift the MDD thermal histories by about 25 °C, making the 1400–1200 Ma thermal histories between K-feldspar and biotite more compatible. However, it is difficult to reconcile the substantial difference in the 1000–800 Ma range. Dotson's (1994) closure temperature estimates are based on the physical dimension of each crystal, and using this assumption, one would expect a simple pattern with younger dates near crystal edges and older dates near crystal cores. This is not observed, and Dotson (1994) considered several mechanisms to explain the

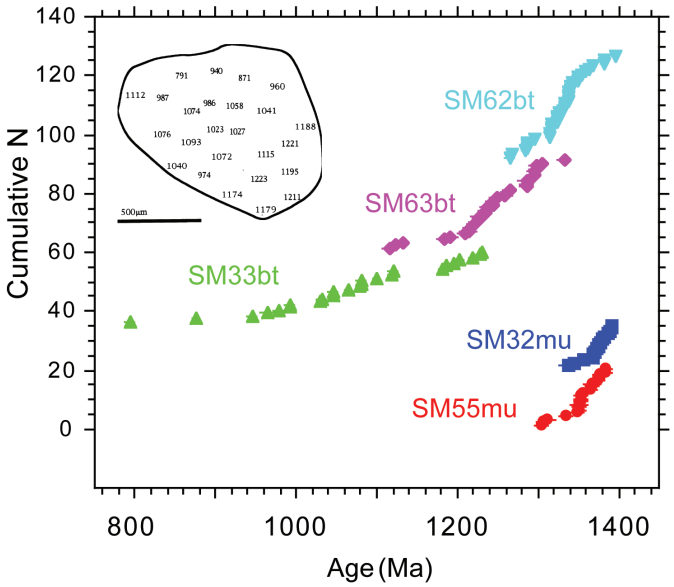


FIGURE 9. Summary of in situ laser probe $^{40}Ar/^{39}Ar$ dates within biotite (bt) and muscovite (mu) crystals from Dotson (1994). Data for each crystal are arranged in increasing age order without spatial context. Muscovite crystals exhibit the least internal date variation and are overall consistent with the age-spectrum data reported here. Biotite grains show substantial internal age variation that likely represents long-term crustal residence between about 275 and 325 °C. Inset is biotite crystal SM33bt showing an example of the spatial distribution of dates within the grain. The lack of a clear relationship between young dates near crystal edges and older dates near crystal cores are discussed in the text. These complex internal age distributions have important implications for bulk age-spectrum interpretations and thermal history analysis; however, it is difficult to reconcile biotite dates near 800 Ma and representing temperatures near 300 °C with the K-feldspar MDD results.

age patterns; for instance, the existence of "fast-path" internal diffusion boundaries, chemical zonation, vacancy distributions, and whether the grains may have been broken, thereby potentially allowing original crystal cores to be exposed at the analyzed crystal rim.

Harrison et al. (1985) suggested that large biotite grains were internally compartmentalized into about 100 µm radii diffusion boundaries, thereby suggesting the closure temperature was not a simple function of crystal size. Variable subgrain diffusion boundaries within the Sandia granite biotite grains could explain the non-uniform spatial distribution of dates reported by Dotson (1994) and significantly reduce the calculated closure temperatures. This reduction, perhaps by as much as 50 °C, would provide good alignment between the K-feldspar and biotite-derived thermal histories between about 1400 and 1200 Ma.

Lastly, the complex internal age distributions measured by Dotson (1994) within the biotites provide a good explanation for the complexity of the age spectra shown in Figure 5. The step-heating approach appears to only partially homogenize these internal variations, resulting in somewhat chaotic age spectra. The Dotson (1994) data also support choosing the oldest step as a minimum estimated time for the onset of argon retention.

Another thermochronometer, zircon (U-Th)/He (ZHe), has an overlapping closure temperature with argon in K-feldspar. Ricketts et al. (2021) modeled ZHe data in HeFTy using the K-feldspar constraints for the Sandia Mountains reported here and other Precambrian locations in the southern Rocky Mountains. This modeling involved assigning constraint boxes based on both the K-feldspar MDD model and firm geologic information to constrain good and acceptable paths, and a best-fit path that also satisfies the ZHe data. As shown in Figure 10, the envelope of 7 good paths from Ricketts et al. (2021) intersects our preferred paths at the red ovals of Figure 8 (as the models were required to do by the constraint boxes), but the envelope between 250 and 150 °C is approximately 100 °C cooler than our preferred model. These models also showed cooling segments in some of the acceptable paths at ~500 Ma, but the ZHe data do not contribute firm additional constraints for the T–t path in the interval 800 to 300 Ma. A similar study in the Grand Canyon (Thurston et al., 2024) that applied joint modeling of argon-K-feldspar and ZHe in QtQT also showed that the Ar MDD models provide the firmest constraints for the Precambrian segments of the joint thermal histories. Because the K-feldspar age spectra record Precambrian ages, they appear to provide the most accurate thermal history for these types of joint models. The bulk cooling age of the zircon is commonly much younger than the part of the thermal history it is attempting to constrain, and thus uncertainties in model parameters, such as the effects of radiation damage, are likely contributing to uncertainty in the derived thermal history.

CONCLUSIONS

Based on new $^{40}Ar/^{39}Ar$ muscovite and biotite data and republishing a single K-feldspar result, our data for the sub-Pennsylvanian Great Unconformity in the Sandia Mountains supports a multi-stage erosion hypothesis for ~5 km (~3.1 mi) of denudation between 1.0 and 0.8 Ga. This depth is inferred from thermochronology temperature data with an assumed geothermal gradient (25–30 °C/km). In agreement with Heizler et al. (1997) and Sanders et al. (2006), this is interpreted to be due to west-side-up uplift of the Rocky Mountains relative to the Great Plains as a far-field inboard effect of the Grenville orogen and assembly of Rodinia. This cooling event in the Rocky Mountains predated the Rodinia breakup ~750 Ma (Delucia et al., 2018) and the proposed 720–650 Ma Snowball Earth erosion (Keller et al., 2019). Removal of the second 5 km (3.1 mi) took place in one or more events (3–6 on Fig. 8), including a possible major component during the Ancestral Rocky Mountain orogeny. The $^{40}Ar/^{39}Ar$ K-feldspar data, with a few young ages in initial heating steps, also show reheating to ~150 °C by burial of ~5 km (3.1 mi) of 300–35 Ma rocks and are compatible with the AFT and AHe thermochronology that shows rapid cooling after ~20 Ma due to uplift and erosion of the post-Mississippian stratigraphic section off the Sandia Mountain rift flank. This paper demonstrates how thermochronometry can help resolve what happened during the time of the "missing" rock at Great Unconformities, and that combined data from multiple thermochronometers provides the best constraints.

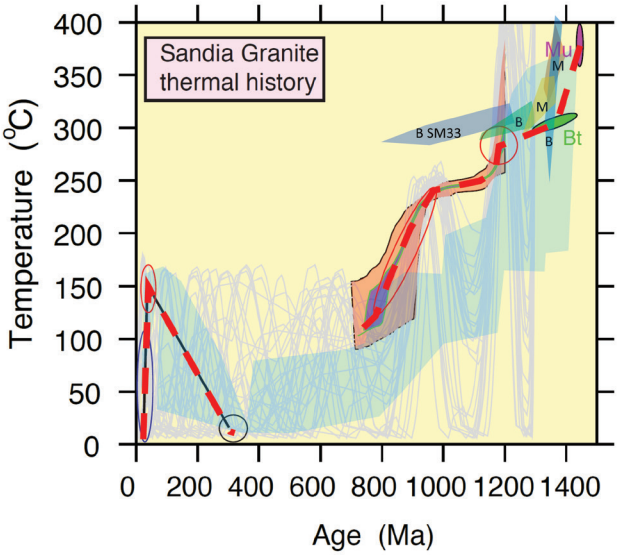


FIGURE 10. Comparison of our preferred cooling path (red dashed line) with diffusion modeling of micas from Dotson (1994); models are compatible except for biotite BSM33 (Fig. 9), which is about 50 °C hotter from 1.1 Ga to 0.8 Ga. Envelope of 7 "good" paths from the ZHe model (blue) are about 50–100 °C cooler and provide little constraint on the poorly resolved 800–300 Ma interval.

ACKNOWLEDGEMENTS

This work is an extension of thermochronology in unpublished master's theses by Lisa Gaston at New Mexico Institute of Mining and Technology and Emily Dotson at Massachusetts Institute of Technology. This manuscript benefited from the

thoughtful reviews of Kent Condie and Rebecca Flowers. We thank Eric Kirby for his longtime efforts on the Sandia granite and for providing the "K-series" samples. Financial support was partly from NSF grant EAR–9902955 (Collaborative Research: Great Unconformity of the Southwestern U.S.A.: Ar K-feldspar thermochronologic and structural studies of a billion years of regional exhumation, awarded to Karlstrom and Heizler, University of New Mexico, between July 15, 1999, and June 30, 2002).

REFERENCES

Amarante, J.F.A., Kelley, S.A., Heizler, M.T., Barnes, M.A., Miller, K.C., and Anthony, E.Y., 2005, Characterization and age of the Mesoproterozoic Debaca sequence in the Tucumcari Basin, New Mexico, *in* Karlstrom, K.E., and Keller, G.R., eds., The Rocky Mountain Region—An Evolving Lithosphere: Tectonics, Geochemistry, and Geophysics: American Geophysical Union Geophysical Monograph 154, p. 185–199. https://doi.org/10.1029/154GM13

Amato, J. M., and Mack, G. H., 2012, Detrital zircon geochronology from the Cambrian- Ordovician Bliss Sandstone, New Mexico: Evidence for contrasting Grenville-age and Cambrian sources on opposite sides of the Transcontinental Arch: Geological Society of America Bulletin, v.124, p. 1826–1840. https://doi.org/10.1130/B30657.1

DeLucia, M.S., Guenthner, W.R., Marshak, S., Thomson, S.N., and Ault, A.K., 2017, Thermochronology links denudation of the Great Unconformity surface to the supercontinent cycle and snowball Earth: Geology, v. 46, p. 167–170. https://doi.org/10.1130/G39525.1

Dotson, E., 1994, Argon Diffusion Gradients in Micas and Implications for the Thermal History of the Sandia Pluton [unpublished Master Thesis], Massachusetts Institute of Technology, 80 p.

Dodson, M.H., 1973, Closure Temperature in Cooling Geochronological and Petrological Systems: Contributions to Mineralogy and Petrology, v. 40, p. 259–247. https://doi.org/10.1007/BF00373790

Dutton, C.E., 1882, Tertiary history of the Grand Cañon District, with atlas: U.S. Geological Survey Monograph 2, scale 1: 250,000, 264 p. https://doi .org/10.3133/m2.

Grove, M., and Harrison, T.M., 1996, ^{40}Ar* diffusion in Fe-rich biotite: American Mineralogist, v. 81, no. 7–8, p. 940–951. https://doi.org/10.2138/am-1996-7-816.

Harrison T. M., Duncan I., and McDougall I., 1985, Diffusion of ^{40}Ar in biotite – temperature, pressure and compositional effects: Geochimica Cosmochimica Acta, v. 49, p. 2461–2468. https://doi.org/10.1016/0016-7037(85)90246-7

Harrison, T.M., Celerier, J., Aikman, A., Hermann, J., and Heizler, M.T., 2009, Diffusion of ^{40}Ar in muscovite: Geochimica Cosmochimica Acta, v. 73, p. 1039–1051. https://doi.org/10.1016/j.gca.2008.09.038

Heizler, M.T., Lux, D.R., and Decker E.R., 1988, The age and cooling history of the Chain of Ponds and Big Island Pond plutons and the Spider Lake granite, west-central Maine and Quebec: American Journal of Science, v. 288, p. 925–952. https://doi.org/10.2475/ajs.288.9.925

Heizler, M.T., Ralser, S., and Karlstrom, K.E., 1997, Late Proterozoic (Grenville ?) deformation in central New Mexico determined from single crystal muscovite $^{40}Ar/^{39}Ar$ age spectra: Precambrian Research, v. 84, 1–15. https://doi.org/10.1016/S0301-9268(96)00053-8

Hodges, K. V, Hames, W. E., and Bowring, S.A., 1994, $^{40}Ar/Ar^{39}Ar$ age gradients in micas from a high-temperature-low-pressure metamorphic terrain: Evidence and implications for the interpretation of age spectra: Geology, v. 22, p. 55–58. https://doi.org/10.1130/0091-7613(1994)022%3C0055:AAAGIM%3E2.3.CO;2

Holland, M.E., Grambling, T.A., Karlstrom, K.E., Jones, J.V., III, Nagotko, K.N., and Daniel, C.G., 2020, Geochronologic and Hf-isotope framework of Proterozoic rocks from central New Mexico, USA: Formation of the Mazatzal crustal province in an extended continental margin arc: Precambrian Research, v. 347. https://doi.org/10.1016/j.precamres.2020.105820

Holland, M.E., Mohr, M., Schmitz, M., Madronich, L., and Karlstrom, K., 2024, Source-to-sink tandem geochronology reveals tectonic influences on the Cambrian Transcontinental Arch of Laurentia: Terra Nova, v. 36, p. 161–169. https://doi.org/10.1111/ter.12692

Karlstrom, K.E., Hagadorn, J., Gehrels, G.G., Mathews, W., Schmitz, M., Madronich, L., Mulder, J., Pecha, M., Geisler, D., and Crossey, L.J., 2018, Cambrian Sauk transgression in the Grand Canyon region redefined by detrital zircons: Nature Geoscience, v. 11, p. 438–443. https://doi.org/10.1038/s41561-018-0131-7

Karlstrom, K.E., and Timmons, J.M., 2012, Many unconformities make one 'Great Unconformity', *in* Timmons, J.M., and Karlstrom, K.E., eds., Grand Canyon Geology: Two Billion Years of Earth's History: Geological Society of America Special Paper 489, p. 73–79, https://doi .org /10 .1130 /2012 .2489(04).

Keller, C.B., et al., 2019, Neooproterozoic glacial origin of the Great Unconformity: Proceedings of the National Academy of Science, v. 116, p. 1136–1145.

Kirby, E., Karlstrom, K.E., and Andronicus, 1995, Tectonic setting of the Sandia pluton: an orogenic 1.4 Ga granite in New Mexico: Tectonics, v. 14, p. 185–201. https://doi.org/10.1029/94TC02699

Leary, R.J., Umhoefer, P., Smith, M.E., and Riggs, N., 2017, A three-sided orogeny: A new tectonic model for Ancestral Rocky Mountain uplift and basin development: Geology, v. 45, p. 735–738. https://doi.org/10.1130/G39041.1.

Lovera, O. M., Richter, F. M., and Harrison T.M., 1989, $^{40}Ar/^{39}Ar$ geothermometry for slowly cooled samples having a distribution of diffusion domain sizes: Journal Geophysical Research, v. 94, p. 17,917–17,935. https://doi.org/10.1029/JB094iB12p17917

Mohr, M.T., Schmitz, M.D., Swanson-Hysell, N.L., Karlstrom, K.E., Macdonald, F.A., Holland, M.E., Zhang, Y., and Anderson, N.S., 2024, High-precision U-Pb geochronology links magmatism in the southwestern Laurentia large igneous province and midcontinent rift: Geology, v. 52, p. 193–198. https://doi.org/10.1130/G51786.1

Ricketts, J.W., Kelley, S.A., Karlstrom, K.E., Schmandt, B., Donahue, M.S., and van Wijk, J., 2016, Synchronous opening of the Rio Grande rift along its entire length at 25–10 Ma supported by apatite (U-Th)/He and fission-track thermochronology, and evaluation of possible driving mechanisms: Geological Society of America Bulletin, v. 128, p. 397–424. https://doi.org/10.1130/B31223.1

Ricketts, J.W., Roiz, J., Karlstrom, K.E., Guenthner, W.R., Heizler, M.T., and Timmons, J.M., 2021, Tectonic origin of basement exhumation in the southern Rocky Mountains (United States): The power of combined zircon (U-Th)/He and K-feldspar $^{40}Ar/^{39}Ar$ thermochronology: Geology, v. 49, no. 10, p. 1187–1192. https://doi.org/10.1130/G49141.1.

Sanders, R.E., Heizler, M.T., and Goodwin, L.B., 2006, $^{40}Ar/^{39}Ar$ thermochronology constraints on the timing of Proterozoic basement exhumation and fault ancestry, southern Sangre de Cristo Range, New Mexico: Geological Society of America Bulletin, v. 118, p. 1489–1506. https://doi.org/10.1130/B25857.1.

Timmons, J. M., Bloch, J., Fletcher, K., Karlstrom, K.E., Heizler, M.T., and Crossey, L. J., 2012, The Grand Canyon Unkar Group: Mesoproterozic basin formation in the continental interior during supercontinent assembly, *in* Timmons, J.M., and Karlstrom, K.E., eds., Grand Canyon Geology Two Billion Years of Earth's History: Geological Society of America Special Paper 489, p. 25–48. https://doi.org/10.1130/2012.2489(02)

Thurston, O.G., Guenthner, W.R., Karlstrom, K.E., Heizler, M.T., Ricketts, J.W., and McDannell, K., 2024, Deep-time thermal history of the Great Unconformity in the Grand Canyon, USA: Combined zircon (U-Th)/He and K-feldspar $^{40}Ar/^{39}Ar$ thermochronometers: Geological Society of America Bulletin, v. 136, p. 4815–4835. https://doi.org/10.1130/B37358.1

Whitmeyer, S.J., and Karlstrom, K.E., 2007, Tectonic model for the Proterozoic growth of North America: Geosphere, v. 3, p. 220–259. https://doi.org/10.1130/GES00055.1

Appendices can be found at
https://nmgs.nmt.edu/repository/index.cfml?rid=2026001



Sandia “stonehenge” is a natural arrangement of weathered Sandia granitic corestones in the Sandia Mountains. Photograph courtesy of Stan Davis.